arXiv:1511.07042v1 [math.NA] 22 Nov 2015

BOOTSTRAP MULTIGRID FOR THE SHIFTED LAPLACE-BELTRAMI EIGENVALUE PROBLEM

JAMES BRANNICK AND SHUHAO CAO

Abstract. This paper introduces both a two-grid and a bootstrap multigrid finite element approximation to the Laplace-Beltrami (surface Laplacian) eigen-problem on a closed surface. The proposed multigrid method is suitable for solving problems with eigenvalues having large multiplicity, computing interior eigenvalues, and solving the shifted indefinite eigen-problem. Convergence analysis is carried out for a simplified two-grid algorithm and numerical experiments are presented to illustrate the basic components and ideas behind the overall bootstrap multigrid approach.

1. Introduction

We consider developing multigrid methods for the surface finite element (SFEM) approximation to the Laplace-Beltrami eigen-problem

$$-\Delta_\Gamma u = \lambda u, \tag{1.1}$$

where Δ_Γ denotes the Laplace-Beltrami operator on a 2-dimensional, smooth, orientable, and closed surface Γ. $\lambda \in \mathbb{R}^+$ is the eigenvalue, and $u : \Gamma \to \mathbb{R}$ denotes the associated eigenfunction. Letting

$$a(u,v) := \int_\Gamma \nabla_\Gamma u \cdot \nabla_\Gamma v \, dS, \quad \text{and} \quad b(u,v) = \int_\Gamma uv \, dS, \tag{1.2}$$

the variational formulation of (1.1) is as follows: find $u \in H^1(\Gamma)$ and $\lambda \in \mathbb{R}^+$ such that

$$a(u,v) = \lambda b(u,v), \quad \text{for any } v \in H^1(\Gamma). \tag{1.3}$$

For a closed surface, it is known that the first eigenvalue of $-\Delta_\Gamma$ is always 0 with a constant eigenfunction, and the integral of eigenfunction u associated with a nonzero eigenvalue on the whole surface is 0. Instead of working on recovering the eigenpairs with the "zero average" compatibility condition, it is convenient to work on approximating eigenfunctions in $H^1(\Gamma)$ as in (1.3) and set all eigenfunctions associated with a nonzero eigenvalue perpendicular to the first eigenfunction with 0 eigenvalue.

For surface finite element method (SFEM), a summary of existing works on SFEM is found in [14]. The linear algebra aspects of these problems, e.g., the condition number of the stiffness and mass matrices on certain triangulations, are discussed in [22]. Recently in [27] Chen et. al. studied the path recovery techniques for surface finite elements.

For the Laplace eigen-problem on the plane, a two-grid eigensolver was proposed by Xu [28], and later improved by Hu and Zhou in [16]. A similar approach was designed for the Maxwell eigen-problem in [29]. However, there is no known two-grid eigensolver for the Laplacian-Beltrami operator on surfaces in the finite element setting. Extending the two-grid methods on

This work was supported in part by the National Science Foundation under grant DMS-1320608.

the plane to a multigrid approach for the Laplace-Beltrami operator on Γ is one focus of this paper. The extension we consider involves a suitable geometric projection from coarse spaces to fine spaces defined on a sequence of refined and non-nested meshes.

Though two-grid methods do provide improvements compared to single-grid methods, they have two main drawbacks in practice. First, two-grid methods in general are not optimal as the mesh spacing goes to zero since the coarse eigen-problem needs to be solved with sufficient accuracy. Second, to resolve high eigenmodes (i.e., corresponding to large eigenvalues) the coarse mesh used in the two-grid method must be fine enough. We observe a "loss of spectra" phenomena for the two-grid methods when the coarse mesh is not fine enough and overcome this issue by using a bootstrap multilevel approach from [3].

In [5], multilevel analogues of the two-grid solvers noted above are developed. Specifically, the paper develops multilevel approaches for nearly singular elliptic problems and eigen-problems. It should be noted that these methods preserve the components in the eigenspace of the smallest eigenvalue of (1.3). Thus, they can be used only to compute eigenpairs in some small neighborhood of the smallest eigenvalue.

In a recent paper by Lin and Xie ([19]), another multilevel approach was developed. The main ingredient in their method is to solve the coarse eigen-problem in an enriched space. This enrichment is achieved by including an extra function obtained by solving a positive definite source problem on a finer mesh. Then, this two-grid correction scheme is used repeatedly to span multiple levels, resembling the bootstrapping procedure developed in [3]. In the setting of this paper, the source problem that is solved is indefinite so that using optimal solvers such as multigrid may become problematic. As we show numerically in this paper, it is not necessary to solve this indefinite problem directly and a few sweeps of an iterative solver suffices to obtain an optimal multigrid algorithm. In certain cases, the shift can even be moved to the right hand side using an interpolated coarse approximation to the eigenfunction of interest.

Moreover, it is known that the Laplace-Beltrami eigenvalue has very high multiplicity for closed surfaces (e.g. see [26] Chapter 3). For example, for the Laplacian-Beltrami operator on the 2-sphere, the number of linearly independent eigenfunctions associated with l-th distinct eigenvalue $\lambda = l(l+1)$ is $2l+1$. Thus, an approach that enriches the coarsest space with a subspace of linearly independent functions is needed for this model problem. The approach that we consider here is given by the bootstrap multilevel eigensolver proposed in [3]. Therein, a bootstrap algebraic multigrid (BAMG) process is proposed that can be used for computing multiple (smooth and oscillatory) eigenpairs for symmetric and positive definite matrices. The BAMG method was later extended to the non-Hermitian (or Hermitian and indefinite) Wilson Dirac system [4]. The main component of the bootstrap approach is its enrichment of the coarsest space with multiple functions obtained from solving source problems on finer meshes with appropriately chosen right hand side.

The idea to enrich the coarse space in designing eigensolvers goes back to the papers [17] and [20]. The authors also analyze an iterative method for computing the smallest eigenpair under the somewhat restrictive condition that the initial guess of the eigenfunction is sufficiently close to the smallest one, namely that it yields a eigenvalue approximation that lies between the smallest and second smallest eigenvalues. In [6] the method from [17] is extended to both two-grid and multigrid methods and an algorithm for computing a given number of the smallest eigenpairs is presented. The paper also presents a convergence theory with less restrictive assumptions on the initial guess.

In this paper, we develop a geometric bootstrap multigrid solver (BMG) for the surface finite element discretization of the shifted Laplace-Beltrami eigen-problem. The approach we

propose can be seen as a generalization of the approaches proposed in [17, 20, 6, 19] in that we enrich the coarse space with a subspace, instead of a single eigenfunction, and we consider also shifted and indefinite Helmholtz type eigen-problems. Alternatively, it can be viewed as a simplification of the BAMG algorithm since we use the finite element spaces to explicitly define the components of the multilevel method, including the enriched coarsest space eigen-problem.

This paper is organized as follows. In Section 2, we provide some preliminary results and notations. In Section 3, we introduce the standard two-grid method for solving elliptic eigen-problems that was introduced in [28] and further developed in [16]. In addition, we prove the convergence of the method for the model Laplace-Beltrami eigen-problem on surfaces. In Section 4, we introduce a finite element bootstrap multigrid method for the same problem. Section 5 contains results of numerical experiments for both the two-grid and multigrid methods applied to the model problem on the 2-sphere $\mathbb{S}^2$.

2. Notation and Preliminary results

Approximating (1.3) with the finite element method requires two discrete approximations. First, a polygonal surface is generated to approximate Γ, where the surface consists of only 2-simplices (triangles), i.e., a triangulation is constructed with $\mathcal{T}_h$ being the set of these triangles. Second, a finite element discretization is constructed to approximate the continuous eigen-problem on the discrete surface. The surface gradient on a 2-dimensional smooth orientable surface that can be embedded into $\mathbb{R}^3$ is defined as follows:

Definition 2.1. For any $f \in H^1(\Gamma)$, define the surface gradient operator $\nabla_\Gamma : H^1(\Gamma) \to (L^2(\Gamma))^3$ as:

$$(\nabla_\Gamma f)(\boldsymbol{x}) := \lim_{\boldsymbol{y}\to\boldsymbol{x}} \boldsymbol{n}(\boldsymbol{x}) \times \big(\nabla \widetilde{f}(\boldsymbol{y}) \times \boldsymbol{n}(\boldsymbol{x})\big), \tag{2.1}$$

where $\widetilde{f}$ is the smooth extension of f to a 3-dimensional neighborhood Ω of Γ, $\nabla : H^1(\Omega) \to (L^2(\Omega))^3$ is the weak gradient operator in $\mathbb{R}^3$, and $\boldsymbol{n}(\boldsymbol{x})$ is the unit normal pointing to the outside of this closed surface at point $\boldsymbol{x}$. The Laplace-Beltrami operator Δ_Γ is defined in a distributional sense:

$$\langle \Delta_\Gamma f, g\rangle = \int_\Gamma (\Delta_\Gamma f) g \, dS := \int_\Gamma \nabla_\Gamma f \cdot \nabla_\Gamma g \, dS, \quad \forall g \in C^\infty(\Gamma). \tag{2.2}$$

For a more detailed definition and the technicalities that arise when defining a differential operator on surfaces, we refer to [10, 14, 27].

2.1. The eigen-problem on the discrete surface.

Let $\Gamma_h = \cup_{T\in\mathcal{T}_h} T$ be a polygonal surface that approximates the continuous surface Γ and assume Γ_h is quasi-uniform and regular. The mesh size is then defined as the maximum of the diameter of all the triangles: $h := \max_{T\in\mathcal{T}_h} \operatorname{diam} T$. Further, the set of all vertices is denoted by $\mathcal{N}_h$. For any $\boldsymbol{z} \in \mathcal{N}_h$, $\boldsymbol{z} \in \Gamma$, i.e., any vertex in the triangulation lies on the original continuous surface Γ.

Note that the surface gradient on a smooth surface in Definition 2.1 carries over naturally to a discrete surface Γ_h: the unit normal $\boldsymbol{n}$ is now a piecewise constant vector $\boldsymbol{n}_T$ on each triangle T. For ease of notation, the surface gradient ∇_{Γ_h} on Γ_h and on Γ will both be denoted by ∇_Γ, where the definition should be clear from the context. With these definitions the bilinear form of (2.2) on Γ_h is as follows

$$a_h(u,v) := \int_{\Gamma_h} \nabla_\Gamma u \cdot \nabla_\Gamma v \, dS, \quad \text{and} \quad b_h(u,v) := \int_{\Gamma_h} uv \, dS. \tag{2.3}$$

The fact that this discrete surface is piecewise linear, which is a $C^{0,1}$-surface, implies that the Sobolev space $H^1(\Gamma_h)$ is well-defined on this surface (see [13]).

The continuous variantional formulation for the eigen-problem on the discrete surface Γ_h is now given by: find $u \in H^1(\Gamma_h)$ and $\bar{\lambda} \in \mathbb{R}^+$ such that

$$a_h(u,v) = \bar{\lambda}\, b_h(u,v), \qquad \text{for any } v \in H^1(\Gamma_h). \tag{2.4}$$

Using the Poincaré inequality and the geometric error estimate between (2.2) and (2.3) (e.g. see [14] Section 4), it follows that if the mesh is sufficiently fine (required for the coercivity), then for any $u, v \in H^1(\Gamma_h)/\mathbb{R}$

$$\begin{aligned} a_h(u,v) &\lesssim \|u\|_{H^1(\Gamma_h)} \|v\|_{H^1(\Gamma_h)}, \\ \text{and } a_h(u,u) &\gtrsim \|u\|_{H^1(\Gamma_h)}. \end{aligned} \tag{2.5}$$

Throughout this article, $x \lesssim y$ and $z \gtrsim w$ are used for convenience to represent $x \leq c_1 y$ and $z \geq c_2 w$ respectively, where c_1 and c_2 are two constants independent of the mesh size h and eigenvalues. The constants in these inequalities may in certain cases depend on specific eigenvalue(s) and when such dependence exists, it will be stated explicitly.

Since every closed surface is compact, it follows from spectrum theory of the Laplacian-Beltrami operator on compact surfaces (e.g. see [7]) that the eigenvalues $\{\bar{\lambda}_i\}_{i=0}^{\infty}$ for problem (2.4) form a discrete sequence, with no accumulation point:

$$0 = \bar{\lambda}_0 < \bar{\lambda}_1 \leq \bar{\lambda}_2 \leq \cdots \to \infty.$$

Moreover, the eigenfunctions ϕ_k associated $\bar{\lambda}_k$ are orthogonal in the sense that $b_h(\phi_i, \phi_j) = \delta_{ij}$.

Let $M(\bar{\lambda})$ be the eigenspace spanned by all the eigenfunctions associated with eigenvalue $\bar{\lambda}$ for the continuous eigen-problem (2.4) defined on the triangulation $\mathcal{T}_h$:

$$M(\bar{\lambda}) := \{u \in H^1(\Gamma_h) : a_h(u,v) = \bar{\lambda} b_h(u,v), \forall v \in H^1(\Gamma_h)\}. \tag{2.6}$$

Similarly, the eigenspace for the continuous eigen-problem on the continuous surface Γ is given by

$$M(\lambda) := \{u \in H^1(\Gamma) : a(u,v) = \lambda b(u,v), \forall v \in H^1(\Gamma)\}. \tag{2.7}$$

2.2. **Finite Element Approximation.** We consider the finite element approximation to problem (2.4) that uses piecewise affine linear polynomials which are continuous across the inter-element edges as the test function and trial function spaces denoted by V_h:

$$V_h = \{\phi_h \in C^0(\Gamma_h) : \phi_h\big|_T \in P^1(T)\ \forall T \in \mathcal{T}_h\}. \tag{2.8}$$

The finite element approximation to problem (2.4) is then: find $u_h \in V_h$ and $\lambda_h \in \mathbb{R}^+$ such that

$$a_h(u_h, v) := \int_{\Gamma_h} \nabla_\Gamma u_h \cdot \nabla_\Gamma v \, dS = \lambda_h \int_{\Gamma_h} u_h v \, dS, \qquad \text{for any } v \in V_h. \tag{2.9}$$

Note that the finite element approximation to problem (2.9) on the discrete triangulated surface Γ_h approximates the continuous eigen-problem (2.4) on the discrete surface. The connection between the finite element solution on Γ_h and the continuous solution on the surface Γ is established through a bijective lifting operator (see e.g. [10]).

It is assumed that there is a bijective mapping between any triangle $T \subset \Gamma_h$ to a curvilinear triangle on Γ, then for any $v \in H^1(\Gamma_h)$, its lifting $\widetilde{v}$ to the continuous surface Γ can be defined as follows: for any point $\boldsymbol{x} \in \Gamma_h$, there is a unique point $\widetilde{\boldsymbol{x}} \in \Gamma$, such that

$$\widetilde{\boldsymbol{x}} + d(\boldsymbol{x})\boldsymbol{n}(\widetilde{\boldsymbol{x}}) = \boldsymbol{x}, \quad \text{and} \quad \widetilde{v}\big(\widetilde{\boldsymbol{x}}\big) = v(\boldsymbol{x}), \tag{2.10}$$

where $d(\boldsymbol{x})$ is the signed distantce to Γ at point $\boldsymbol{x} \in \Gamma_h$, being positive when $\boldsymbol{x}$ is outside of the closed surface Γ, with $|d(\boldsymbol{x})| = \min_{\boldsymbol{y}\in\Gamma} |\boldsymbol{x}-\boldsymbol{y}|$. When all the vertices of Γ_h lie on the continuous surface Γ with C^m-smoothness ($m \geq 2$), it is known that $\|d\|_{L^\infty(\Gamma_h)} \lesssim h^2$.

Conversely, through this lifting bijection, for any $v \in H^1(\Gamma)$, its restriction on the discrete surface Γ_h can be defined as $\bar{v}$ such that for any $\boldsymbol{x} \in \Gamma_h$

$$\bar{v}(\boldsymbol{x}) = v\big(\boldsymbol{x} - d(\boldsymbol{x})\boldsymbol{n}(\widetilde{\boldsymbol{x}})\big). \tag{2.11}$$

In [13], the following lemma comparing the H^1-seminorms between the original function lying on the discrete surface and the lifting to the continuous surface is proved.

Lemma 2.2. *If $\|d\|_{L^\infty(\Gamma_h)} \lesssim h^2$, then for any $v \in H^1(\Gamma_h)$*

$$\begin{aligned} &(1-ch^2)\,|u|_{H^1(\Gamma_h)} \leq |\widetilde{u}|_{H^1(\Gamma)} \leq (1+ch^2)\,|u|_{H^1(\Gamma_h)}\,, \\ \textit{and}\quad &(1-ch^2)\,\|u\|_{L^2(\Gamma_h)} \leq \|\widetilde{u}\|_{L^2(\Gamma)} \leq (1+ch^2)\,\|u\|_{L^2(\Gamma_h)}\,. \end{aligned} \tag{2.12}$$

Let $\delta_h(\bar{\lambda})$ measure the approximation, under the H^1-seminorm, of the discrete space V_h to the continuous eigenspace $M(\bar{\lambda})$ on the discrete triangulated surface Γ_h:

$$\delta_h(\bar{\lambda}) := \sup_{u\in M(\bar{\lambda})} \inf_{v_h\in V_h} |u - v_h|_{H^1(\Gamma_h)}. \tag{2.13}$$

Using the estimate from the quasi-interpolation of Clément-type as v_h introduced in [9] and extended to surface finite elements in [10], we have $\delta_h(\bar{\lambda}) \lesssim h$. Notice that a standard global Bramble-Hilbert estimate cannot be applied because $H^2(\Gamma_h)$ is not well-defined for a polygonal surface Γ_h. With the lifting (2.10) available, we can define the following quantity as well:

$$\delta_h(\lambda) := \sup_{u\in M(\lambda)} \inf_{v_h\in V_h} |u - \widetilde{v}_h|_{H^1(\Gamma)}. \tag{2.14}$$

The orientability of Γ guarantees that it can be embedded into $\mathbb{R}^3$. In [11], the author establishes the well-known cotangent formulation (e.g. see [21]) approximating the Laplace-Beltrami operator on a surface that can be embedded in $\mathbb{R}^3$. An a priori estimate is proved for the eigenvalues of the discrete Laplace-Beltrami operator using cotangent formula, namely that the error is bounded by $\|d\|_{L^\infty(\Gamma_h)}$ with a factor related to the magnitude of the eigenvalue λ.

The cotangent formulation of the Laplace-Beltrami operator is known to be equivalent to the linear finite element formulation on the triangulated surface, e.g. [24] points out this relation, and [13] uses it implicitly. Thanks to this bridging result, we can use the a priori estimate from [11] for the eigenvalue approximation problem (2.9) in the following lemma.

Combining the a priori estimates from [1, 11, 13, 18], we have the following a priori estimates for both λ_h and the corresponding eigenfuntions from problem (2.9).

Lemma 2.3. *If the mesh size h is fine enough and all the vertices of Γ_h lie on Γ, then for any λ that is an eigenvalue of problem (1.3) with multiplicity m on Γ, there exist m $\lambda_h^{(k)}$'s that are the eigenvalues of problem (2.9) on Γ_h, and the following estimate holds*

$$|\lambda_h^{(k)} - \lambda| \leq C(\lambda)h^2, \quad \forall 1 \leq k \leq m. \tag{2.15}$$

Moreover, let $M(\lambda_h) = \operatorname{span}\Big\{u_h^{(k)}\Big\}_{k=1}^{m}$, where $u_h^{(k)}$'s are the eigenfunctions associated with λ_h, then for any eigenfunction $u \in M(\lambda)$,

$$\min_{w_h\in M(\lambda_h)} |u - \widetilde{w}_h|_{H^1(\Gamma)} \leq C(\lambda)h. \tag{2.16}$$

Proof. We present a brief proof as follows mainly bridging the results of eigenvalue problem approximations with results for surface finite elements.

Define the elliptic projection $\Pi_h : H^1(\Gamma) \to V_h$ of an eigenfunction u with respect to the inner product $a_h(\cdot,\cdot)$ as follows:

$$a_h\big(\Pi_h u, v\big) = a(u, \widetilde{v}), \quad \forall v \in V_h.$$

Then by a standard estimate from [1], and Lemma 2.2 we have

$$|\lambda_h^{(k)} - \lambda| \leq C(\lambda) \left(\sup_{u \in M(\lambda)} \left| u - \widetilde{\Pi_h u} \right|^2_{H^1(\Gamma)} + ch^2 \right) \leq C(\lambda)\delta_h(\lambda)^2,$$

assuming the mesh is fine enough. Then by the estimate of the Clément-type interpolant in [10] with the $L^\infty(\Gamma_h)$-norm of the metric distortion tensor being 1 plus a higher order term, $\delta_h(\lambda) \lesssim h$, the estimate (2.15) follows.

To prove estimate (2.16), assume that the true eigenvalue λ to be approximated has multiplicity 2. When λ has bigger multiplicity the same proof follows without essential modifications. Suppose the orthogonal finite element approxmations to the eigenpairs are $\left(\lambda_h^{(1)}, u_h^{(1)}\right)$ and $\left(\lambda_h^{(2)}, u_h^{(2)}\right)$ from problem (2.9). Let w_h be the projection of $\Pi_h u$ onto the discrete eigenspace:

$$w_h := \sum_{i=1,2} b_h\big(\Pi_h u, u_h^{(i)}\big)\, u_h^{(i)} = \sum_{i=1,2} \beta_i\, u_h^{(i)}.$$

Then a standard estimate can be obtained as follows, with the modification using the lifting operator estimates in Lemma 2.2:

$$\begin{aligned} &|u - \widetilde{w}_h|_{H^1(\Gamma)} = a(u,u) - 2a(u,\widetilde{w}_h) + a(\widetilde{w}_h, \widetilde{w}_h) \leq \\ &a(u,u) - 2a(u,\widetilde{w}_h) + a_h(w_h, w_h) + ch^2\, |w_h|_{H^1(\Gamma_h)} = \\ &\lambda - 2\lambda b(u,\widetilde{w}_h) + \beta_1^2 \lambda_h^{(1)} + \beta_2^2 \lambda_h^{(2)} + ch^2\, |w_h|_{H^1(\Gamma_h)} \leq \\ &\lambda\, \|u - \widetilde{w}_h\|^2_{L^2(\Gamma)} - \sum_{i=1,2} \beta_i^2 (\lambda - \lambda_h^{(i)}) + c(\lambda) h^2\, \|w_h\|_{H^1(\Gamma_h)}. \end{aligned} \tag{2.17}$$

By a projection argument (e.g. see [1] or [2] Section 8), the following estimate for the L^2-error holds:

$$\|u - \widetilde{w}_h\|^2_{L^2(\Gamma)} \leq \left(1 + \max_{\substack{\lambda_h \neq \lambda_h^{(k)}, \\ k=1,\ldots,m}} \frac{\lambda}{|\lambda - \lambda_h|} \right) \left\| u - \widetilde{\Pi_h u} \right\|^2_{L^2(\Gamma)} \leq C(\lambda) h^2. \tag{2.18}$$

Lastly, using the estimates (2.15) twice for lower order terms in (2.17) yields estimate (2.16) when the mesh is fine enough.

□

3. A Two-Grid Eigensolver

A two-grid algorithm for solving elliptic eigen-problems is given in Algorithm 1 similar to the one in [29]. An important difference in the case of surfaces as considered in this paper, when compared to previous works for the Poisson problem on the plane, is that the projection operators need extra care. This is because when the mesh is refined the finite element space on the coarse mesh is not a subspace of the fine mesh.

Suppose there are a pair of hierarchical meshes, where the fine mesh $\mathcal{T}_h$ is uniformly refined from the coarse mesh $\mathcal{T}_H$. The newly created vertices, which are the midpoints of the edges of $\mathcal{T}_H$, are projected onto the continuous surface Γ. Denote the coarse finite element approximation space (2.8) by V_H and the fine space by V_h. Note that for the finite element approximation problem on surface meshes the natural inclusion $V_H \not\subset V_h$ does not hold even though all vertices from the coarse mesh are defined such that $\mathcal{N}_H$ is a subset of $\mathcal{N}_h$ when refining.

Consider the geometric projection operator $\mathcal{G}_{H\to\widehat{H}}$ such that

$$\widehat{V}_H := \mathcal{G}_{H\to\widehat{H}} V_H \subset V_h. \tag{3.1}$$

The definition of $\mathcal{G}_{H\to\widehat{H}}$ is then given by: for any vertex $\boldsymbol{z} \in \mathcal{N}_h$ on the fine mesh

$$\widehat{w}_H(\boldsymbol{z}) = \mathcal{G}_{H\to\widehat{H}} w_H(\boldsymbol{z}) = \begin{cases} w_H(\boldsymbol{z}) & \text{if } \boldsymbol{z} \in \mathcal{N}_H, \\ \big(w_H(\boldsymbol{z}_{H,1}) + w_H(\boldsymbol{z}_{H,2})\big)/2 & \text{if } \boldsymbol{z} \in \mathcal{N}_h \backslash \mathcal{N}_H, \end{cases} \tag{3.2}$$

where $\boldsymbol{z}$ is obtained from the projection of the midpoints between the coarse mesh vertices $\boldsymbol{z}_{H,1}$ and $\boldsymbol{z}_{H,2}$.

The prolongation operator (or natural inclusion) $\mathcal{P}_{H\to h}$ can then be defined as

$$\mathcal{P}_{H\to h} : V_H \to V_h,\ w_H \mapsto \widehat{w}_H.$$

To define this operator in matrix notation, suppose the finite element approximation spaces have the following nodal basis set

$$V_H = \operatorname{span}\{\phi_{H,i}\}_{i=1}^{N_H}, \text{ and } V_h = \operatorname{span}\{\phi_{h,i}\}_{i=1}^{N_h}.$$

If $w_H = (W^H)^T \Phi^H$, where $\Phi^H = (\phi_{1,H}, \ldots, \phi_{N_H,H})^T$, then the prolongation operator has the following matrix form:

$$\mathcal{P}_{H\to h} w^H = \mathcal{P}_{H\to h}\Big((W^H)^T \Phi^H\Big) = (P^H W^H)^T \Phi^h,$$

where $P^H : \mathbb{R}^{N_H} \to \mathbb{R}^{N_h}$ is the matrix representation of the prolongation operator. Note that here the geometric projection operator is implicitly imposed.

By (3.2), each $\mathcal{P}_{H\to h}\phi_{H,i}$, evaluated at a newly created vertex $\boldsymbol{z} \in \mathcal{N}_h \backslash \mathcal{N}_H$ different from all coarse mesh vertices, coincides with the value of $\phi_{H,i}$ at this point $\boldsymbol{z}$, before being projected onto the continuous surface. The surface finite element prolongation operator consists of the product $\mathcal{P}_{H\to h} = P_{\widehat{H}\to h}\mathcal{G}_{H\to\widehat{H}}$.

Similarly, restriction operator, that interpolates a finite element function on the fine mesh to the coarse mesh is defined as follows:

$$\mathcal{P}_{h\to H} : V_h \to V_H,\ w_h \mapsto \mathcal{I}_h w_h.$$

Here $\mathcal{I}_h$ is any admissible operator from the fine mesh to the coarse mesh and its matrix representation is

$$\mathcal{P}_{h\to H} w^h = \mathcal{P}_{h\to H}\Big((W^h)^T \Phi^h\Big) = (P^h W^h)^T \Phi^H,$$

where $P^h : \mathbb{R}^{N_h} \to \mathbb{R}^{N_H}$ is the matrix representation of the restriction operator. Note that, as before, the interpolation operator admits the left inverse of the geometric projection $\mathcal{P}_{H\to h}$ by construction.

Given these definitions, the two-grid method is defined as follows in Algorithm 1. When multiple levels of meshes are available (V_{h_k} for $k = 1, \ldots, K$ with $K \geq 3$), Algorithm 1 can be naturally extended to be a multilevel method by being applied in a cascading fashion between two adjacent levels. For example, starting from V_{h_1}, when a two-grid eigenpair approximation

(u^{h_2}, λ^{h_2}) is obtained, we set $(u_{h_2}, \lambda_{h_2}) \leftarrow (u^{h_2}, \lambda^{h_2})$. Then step 2 and step 3 in Algorithm 1 are repeated through level 3 to level K, while shift μ is only added into the Rayleigh quotient on the K-th level.

Algorithm 1 A two-grid scheme for approximating an eigenpair near μ.

1: **Coarse grid eigensolve**
Set a fixed shift $\mu \geq 0$, and find (u_H, λ_H) satisfying

$$a_H(u_H, v) - \mu b_H(u_H, v) = \lambda_H b_H(u_H, v), \quad \text{for any } v \in V_H.$$

2: **Fine grid source solve/relax**
Refine $\mathcal{T}_H$ and perform the geometric projection to get $\mathcal{T}_h$, construct V_h, approximate the u^h satisfying an indefinite source problem on $\mathcal{T}_h$:

$$a_h(u^h, v) - (\mu + \lambda_H) b_h(u^h, v) = b_h(\mathcal{P}_{H\to h} u_H, v), \quad \text{for any } v \in V_h, \tag{3.3}$$

maintaining orthogonality to previous eigenfunctions.

3: **Rayleigh quotient**
Compute the eigenvalue approximation on fine mesh

$$\lambda^h = \frac{a_h(u^h, u^h)}{b_h(u^h, u^h)} + \mu.$$

3.1. **Convergence analysis.** The main ingredient in proving convergence of the two-grid method for the Laplace-Beltrami eigen-problem is to bridge the connection between the geometric projection on the surface with existing two-grid convergence results for the Laplace operator on the plane. The error introduced by the projection between non-hierarchical finite element spaces that arises in this setting is accounted for in the final estimate we derive.

We use the following lemmas to obtain the convergence estimate of the two-grid method. Lemma 3.1 (e.g. see [16]) is the stability estimate for the discrete shifted problem.

Lemma 3.1 (Discrete Shift Inf-Sup Condition)**.** *If μ is not an exact eigenvalue to problem (2.9), then there exists a constant $C(\mu)$ such that*

$$\sup_{v \in V_h} \frac{|a_h(u, v) - \mu b_h(u, v)|}{|v|_{H^1(\Gamma_h)}} \geq C(\mu) \, |u|_{H^1(\Gamma_h)} .$$

The following lemma, Lemma 3.2, is an important identity used to prove the rate of convergence for the approximation of a certain eigenvalue (e.g. see [1]).

Lemma 3.2. *Let $(\lambda, u) \in \mathbb{R}^+ \times H^1(\Gamma)$ be an eigenpair for problem (1.3), then for any $w \in H^1(\Gamma) \backslash \{0\}$*

$$\frac{a(w, w)}{b(w, w)} - \lambda = \frac{a(w - u, w - u)}{b(w, w)} - \lambda \frac{b(w - u, w - u)}{b(w, w)}. \tag{3.4}$$

Aside from $\delta_h(\lambda)$ in (2.14) which measures of the approximability of the discrete space V_h to the eigenspace $M(\lambda)$, set

$$\eta(h) = \sup_{f \in H^1(\Gamma_h), |f|_{H^1} = 1} \inf_{v \in V_h} |Tf - v|_{H^1(\Gamma_h)} , \tag{3.5}$$

where the operators T act on an $H^{-1}(\Gamma_h)$ functionals to get an $H^1(\Gamma_h)$ Riesz representation:

$$a_h(Tf, v) = b_h(f, v), \quad \forall f \in H^1(\Gamma_h), \text{and } \forall v \in H^1(\Gamma_h). \tag{3.6}$$

Now, using Lemma 3.1 together with Lemma 3.2, the following lemma from [16] can be proved for the convergence of the two-grid method.

Lemma 3.3. *Assume that $(\lambda_h, u_h) \in \mathbb{R}^+ \times H^1(\Gamma_h)$ are obtained from the two-grid Algorithm 1 with $V_H \subset V_h$, then for some eigenfunction $u \in M(\lambda)$, the error estimates are*

$$\begin{aligned} &\min_{\alpha\in\mathbb{R}} \|u - \alpha u_h\|_{H^1(\Gamma_h)} \le C\Big(\eta(h)\delta_h(\lambda) + \delta_H^2(\lambda)\delta_h(\lambda)\eta(h) + \delta_H^3(\lambda)\eta(H) + \delta_h(\lambda)\Big), \\ &\textit{and} \quad |\lambda - \lambda_h| \le C\Big(\eta^2(h)\delta_h^2(\lambda) + \delta_H^4(\lambda)\delta_h^2(\lambda)\eta^2(h) + \delta_H^6(\lambda)\eta^2(H) + \delta_h^2(\lambda)\Big). \end{aligned} \tag{3.7}$$

This is the known general estimate for the two-grid approximation if the hierarchical coarse and fine finite element spaces are used, i.e. $V_H \subset V_h$. For finite element eigen-problems, one normally assumes that the eigenspace $M(\lambda)$ has certain regularity, e.g., one assumes that $M(\lambda) \subset H^2(\Gamma_h)$ is at least H^2 so that the interpolation estimate goes through for the infima in the definition of $\eta(h)$ and $\delta_h(\lambda)$:

$$\eta(h) = ch, \quad \text{and} \quad \delta_h(\lambda) \le Ch.$$

Then we have the follow estimate

$$\begin{aligned} &\min_{\alpha\in\mathbb{R}} \|u - \alpha u_h\|_{H^1(\Gamma_h)} \le C(\lambda)\Big(h + H^4\Big), \\ &\text{and} \quad |\lambda - \lambda_h| \le C(\lambda)\Big(h^2 + H^8\Big). \end{aligned} \tag{3.8}$$

However, in the surface case we are interest, Lemma 3.3 cannot be directly applied due to the facts that (a) only $H^1(\Gamma_h)$ is well-defined on a piecewise linear triangulation, (b) when refining, the finite element spaces are not hierarchical. Here a modified version of the two-grid convergence proof is presented following [29] in Theorem 3.4, and similar bounds are obtained as (3.8).

This implies that if the mesh sizes are chosen such that $H \lesssim h^{1/4}$, then the optimal linear convergence rate for the eigenfunction and the quadratic convergence for the eigenvalue follow. These two optimal convergence rates depend on the assumption that the coarse mesh is fine enough.

Theorem 3.4 (Convergence of the two-grid method)**.** *Let λ_H be an approximation to the eigenvalue λ of problem (1.3) satisfying the a priori estimate in Lemma 2.3, and assume the eigenpair (λ^h, u^h) is obtained from the two-grid method given in Algorithm 1 with $\mu = 0$. Then there exists an eigenfunction $u \in M(\lambda)$ such that the following estimate holds*

$$\begin{aligned} &\min_{\alpha\in\mathbb{R}} \big|u - \alpha\widetilde{u}_h\big|_{H^1(\Gamma)} \le C(\lambda)\big(h + H^4\big), \\ &\textit{and} \quad |\lambda - \lambda^h| \le C(\lambda)\big(h^2 + H^8\big). \end{aligned} \tag{3.9}$$

Proof. Assume the coarse approximation λ_H is not an eigenvalue of the discrete eigen-problem (2.9) on the fine mesh. Let an auxiliary solution $\widehat{u}^h = (\lambda_h - \lambda_H)u^h$, then it is known that the this $\widehat{u}^h$ satisfies:

$$a_h(\widehat{u}^h, v) - \lambda_H b_h(\widehat{u}^h, v) = (\lambda_h - \lambda_H) b_h(\mathcal{P}_h u_H, v), \quad \text{for any } v \in V_h.$$

Now let (λ_h, u_h) be a true eigenpair that solves problem (2.9) such that $a_h(u_h, v) = \lambda_h b_h(u_h, v)$ for any test function $v \in V_h$. Taking the difference of these two equations yields the error equation for the two-grid method as follows: for any $v \in V_h$

$$a_h(u_h - \widehat{u}^h, v) - \lambda_H b_h(u_h - \widehat{u}^h, v) = (\lambda_h - \lambda_H) b_h(u_h - \mathcal{P}_h u_H, v). \tag{3.10}$$

Applying the discrete inf-sup stability estimate in Lemma 3.1, we have

$$C\left|u_h-\widehat{u}^h\right|_{H^1(\Gamma_h)} \leq \sup_{v\in V_h}\frac{\left|a_h(u_h-\widehat{u}^h,v)-\lambda_H b_h(u_h-\widehat{u}^h,v)\right|}{|v|_{H^1(\Gamma_h)}} = \sup_{v\in V_h}\frac{|(\lambda_h-\lambda_H)b_h(u_h-\mathcal{P}_h u_H,v)|}{|v|_{H^1(\Gamma_h)}}.$$

By the triangle inequality and the a priori estimate from Lemma 2.3, we have

$$|\lambda_h-\lambda_H|\leq|\lambda-\lambda_h|+|\lambda-\lambda_H|\leq C(\lambda)H^2.$$

The proof of the second estimate is done by restricting the true eigenfunction $u\in M(\lambda)$ with its continuous mapping $\bar{u}$ to the discrete surface Γ_h or Γ_H, and using the geometric error estimate in Lemma 2.2:

$$\sup_{v\in V_h}\frac{b_h(u_h-\mathcal{P}_h u_H,v)}{|v|_{H^1(\Gamma_h)}}\leq\sup_{v\in H^1(\Gamma_h)}\frac{b_h(u_h-\bar{u},v)}{|v|_{H^1(\Gamma_h)}}+\sup_{v\in H^1(\Gamma_h)}\frac{b_h(\bar{u}-\mathcal{P}_h u_H,v)}{|v|_{H^1(\Gamma_h)}}\leq$$
$$c_1(\lambda)\eta(h)\left|u_h-\bar{u}\right|_{H^1(\Gamma_h)}+c_2(\lambda)\eta(H)\left|\bar{u}-u_H\right|_{H^1(\Gamma_H)}+c_3\eta(H)H^2.$$

Now for $\eta(h)$ and $\eta(H)$, since on each element T, the eigenfunction is smooth, then by the interpolation estimate in Lemma 2.2 from [10], we have

$$\eta(h)=\sup_{f\in H^1(\Gamma_h),|f|_{H^1}=1}\inf_{v\in V_h}|Tf-v|_{H^1(\Gamma_h)}\leq Ch,$$

where C only depends on the geometry. Using this result and the a priori estimate for the eigenfunction from Lemma 2.3, we have

$$\left|u_h-\widehat{u}^h\right|_{H^1(\Gamma_h)}\leq C(\lambda)H^4.$$

Then using the triangle inequality and again using the geometric error estimate we have,

$$\left|u-\widetilde{\widehat{u}^h}\right|_{H^1(\Gamma)}\leq|u-\widetilde{u}_h|_{H^1(\Gamma)}+c(\lambda)h^2+\left|u_h-\widehat{u}^h\right|_{H^1(\Gamma_h)}\leq C(\lambda)(h+H^4),$$

where h is assumed to be small enough such that the geometric error can be omitted. Lastly, using the fact that $\widehat{u}^h=(\lambda_h-\lambda_H)u^h$ where u^h is the two-grid approximation, we have

$$\lambda^h=\frac{a_h(u^h,u^h)}{b_h(u^h,u^h)}=\frac{a_h(\widehat{u}^h,\widehat{u}^h)}{b_h(\widehat{u}^h,\widehat{u}^h)}.$$

Then by Lemma 3.2 and assuming the eigenfunction is normalized to have unit L^2 norm, and the fact that the geometric error is of higher order, we can get the estimate for the two-grid approximation λ^h to the true eigenvalue:

$$\begin{aligned}|\lambda^h-\lambda|&=\left|\frac{a_h(u^h,u^h)}{b_h(u^h,u^h)}-\lambda\right|\\&\leq\left|a(\widetilde{u}^h,\widetilde{u}^h)-\lambda\right|+\left|a_h(u^h,u^h)-a(\widetilde{u}^h,\widetilde{u}^h)\right|\\&\leq\left|a(\widetilde{u}^h-u,\widetilde{u}^h-u)-\lambda b(\widetilde{u}^h-u,\widetilde{u}^h-u)\right|+Ch^2\\&\leq\left|\widetilde{u}^h-u\right|^2_{H^1(\Gamma)}+\lambda\left\|\widetilde{u}^h-u\right\|^2_{L^2(\Gamma)}+Ch^2\leq C(\lambda)\big(h^2+H^8\big).\end{aligned}$$

□

4. The Bootstrap Multigrid Method

In this section, we propose a finite element BMG (bootstrap multigrid) eigensolver based on the bootstrap algebraic multigrid (BAMG) framework [3]. The basic idea in the bootstrap approach is to continuously enrich the coarse space with computed approximations of the eigenfunctions coming from finer meshes.

4.1. The two-grid bootstrap algorithm.

A two-grid BMG algorithm is outlined in Algorithm 2.

Algorithm 2 A two-grid BMG scheme for approximating eigenpairs near μ using an enriched coarse space.

1: **Coarse grid eigensolve**
Set a coarse grid shift $\mu_H = \mu \geq 0$, find $(u_{H,i}, \lambda_{H,i}) \in V_H \times \mathbb{R}^+$ (for $i = 1, \ldots, N$ where $N \leq \dim V_H$) satisfying

$$a_H(u_{H,i}, v) - \mu_H b_H(u_{H,i}, v) = \lambda_{H,i} b_H(u_{H,i}, v), \quad \text{for any } v \in V_H. \tag{4.1}$$

2: **Choose eigenfunctions for enrichment**
Let the index set for the enrichment candidate eigenfunctions be $\Lambda \subset \{1, \ldots, N\}$, where Λ is related to the eigenmodes of interest, let

$$X_H := \text{span}\{u_{H,i}\}_{i\in\Lambda}. \tag{4.2}$$

3: **Fine grid source solve/relax**
Refine $\mathcal{T}_H$ and perform the geometric projection to get $\mathcal{T}_h$. Relax for $\widetilde{u}_{h,i} \in V_h$, where $i \in \Lambda$, using $u_{H,i} \in X_H$ as the source, in

$$a_h(\widetilde{u}_{h,i}, v) - \mu_H b_h(\widetilde{u}_{h,i}, v) = \lambda_{H,i} b_h(\mathcal{P}_{H\to h} u_{H,i}, v), \quad \text{for any } v \in V_h. \tag{4.3}$$

Then orthogonalize $\widetilde{u}_{h,i}$'s with respect to the inner product $b_h(\cdot,\cdot)$, let the enrichment space contain the orthogonalized source solutions:

$$X_h := \text{span}\{\widetilde{u}_{h,i}\}_{i\in\Lambda}. \tag{4.4}$$

4: **Coarse grid eigensolve in the enriched space**
Set a new shift μ_h. Find $(u_{H,i}, \lambda_{H,i}) \in V_{H,h} \times \mathbb{R}^+$ satisfying, for $i \in \Lambda$:

$$a_{H,h}(u_{H,i}, v) - \mu_h b_{H,h}(u_{H,i} v) = \lambda_{H,i} b_{H,h}(u_{H,i}, v), \quad \text{for any } v \in V_{H,h}, \tag{4.5}$$

where $V_{H,h} := V_H + X_h$ is the enriched coarse space. Update $X_H = \text{span}\{u_{H,i}\}_{i\in\Lambda}$.

In (4.5), the bilinear forms $a_{H,h}(\cdot,\cdot)$ and $b_{H,h}(\cdot,\cdot)$ are defined as follows. Let $w \in V_H + X_h$ be any function such that $w = w_H + w_h$, where $w_H \in V_H$, and $w_h \in X_h$. Then, for any test function $v = v_H + v_h \in V_H + X_h$

$$\begin{aligned} a_{H,h}(w, v) &:= a_H(w_H, v_H) + a_h(\mathcal{P}_{H\to h} w_H, v_h) \\ &\quad + a_h(w_h, \mathcal{P}_{H\to h} v_H) + a_h(w_h, v_h), \\ \text{and} \quad b_{H,h}(w, v) &:= b_H(w_H, v_H) + b_h(\mathcal{P}_{H\to h} w_H, v_h) \\ &\quad + b_h(w_h, \mathcal{P}_{H\to h} v_H) + b_h(w_h, v_h). \end{aligned} \tag{4.6}$$

Problem (4.3) can be written as: find $U^h \in (\mathbb{R}^{N_h})^d$, where d is the dimension of the eigenspace associated with an approximated eigenvalue of interest

$$(A^h - \mu_H M^h)\widetilde{U}^h = \lambda_H M^h (P^H U^H). \tag{4.7}$$

Here A^h and M^h are the stiffness matrix and mass matrix for the degrees of freedom on the fine approximation space V_h, respectively.

And problem (4.5) can be written as the following matrix eigen-problem:

$$(A^{H,h} - \mu_h M^{H,h})U^h = \lambda_h M^{H,h} U^h, \tag{4.8}$$

where the enriched stiffness and mass matrices $A^{H,h}$ and $M^{H,h}$ are in the following block form: letting $Q^H := P^h \widetilde{U}^h$

$$A^{H,h} = \begin{pmatrix} A^H & A^h Q^H \\ (Q^H)^T A^h & (Q^H)^T A^h Q^H \end{pmatrix}, \text{ and}$$

$$M^{H,h} = \begin{pmatrix} M^H & M^h Q^H \\ (Q^H)^T M^h & (Q^H)^T M^h Q^H \end{pmatrix}.$$

The shifts $\mu_H, \mu_h \geq 0$ are added in Algorithm (2) in case the user is interested in a specific range of the eigenvalues. If one is to find all the eigenvalues from the smallest one, the shift can be set as $\mu = 0$ for all enriched coarse eigensolves, and fine source solves.

We remark that in Algorithm (2), the choice of the set of enrichment functions X_H with index set Λ is related to the eigenspace of interest. In the BAMG ([3]) setup, these functions are named as test vectors. In practice, the choice of X_H is very flexible. As an example, consider the simple case that the user wants to recover the l-th eigenmode, $(\lambda_{h,l}, u_{h,l})$, where $1 \leq l \leq \dim V_H$. The coarse eigensolve contains the discrete approximations $\{(\lambda_{H,i}, u_{H,i})\}_{i=1}^{\dim V_H}$ to these eigenmodes. Then the index set for the enrichment eigenfunctions candidates Λ in (4.2) can be chosen as $\{\hat{k} \in \mathbb{Z} : l - m \leq \hat{k} \leq l\}$, where m is greater than or equal to the geometric multiplicity shown in the discrete spectra for the eigenvalue closest to the eigenvalue of interest $\lambda_{H,l}$. Intuitively, this choice is motivated by the fact that the algorithm should "detect" the improvement in the approximations of the eigenmode $(\lambda_{h,l}, u_{h,l})$ of interest.

4.2. **The bootstrap multigrid cycle.** The V-cycle variant of Algorithm 2 is given by incorporating this two-grid method into a multilevel setting, as we outline in Algorithm 3, and illustrate briefly using 3 levels in Figure 1. The algorithm here is a simplified variant of the BAMG approach presented in [3] since the coarse-level systems and the restriction and interpolation operators can be defined using the finite element formulation at hand; in BAMG the restriction and interpolation operators are defined algebraically and the coarse level system is computed using the Galerkin definition.

Comapring with BAMG, the algorithm we present in this paper instead makes use of a sequence of finite element approximation spaces. We assume that a hierarchical sequence of meshes consisting of K triangulations $\widehat{V}_{h_1} \subset \widehat{V}_{h_2} \subset \cdots \subset \widehat{V}_{h_{K-1}} \subset V_{h_K}$ has been constructed, either using uniform refinement or more generally using an adaptive finite element method, then the 1 through $(K-1)$-th levels are geometrically projected onto the K-th level by recursively using (3.2). We note that at the end of a single BMG V-cycle the coarsest space has been enriched by approximations from the finer spaces. The BMG V-cycle also poses itself as an "inverted" V-cycle as the relaxations process as coarse-fine-coarse, in contrast to the conventional fine-coarse-fine V-cycle for a source problem.

Finally, we present the bootstrap full multigrid (BFMG) method in Algorithm 4. Note that in the BFMG algorithm, the final approximation to a certain eigenpair is given by $(u_{h_K}, \lambda_{h_K}) := (\widetilde{u}_{h_K}, \widetilde{\lambda}_{h_K})$.

Algorithm 3 A BMG V-cycle relaxation for approximating eigenpairs between level 1 and level $k \geq 2$.

1: **Coarse grid eigensolve in an enriched space**
For a fixed shift $\mu_{h_{k-1}}$, solve for the coarse grid eigenpairs $(u_{h_{k-1},i}, \lambda_{h_{k-1},i}) \in V_{h_1,h_{k-1}} \times \mathbb{R}^+$ for $i \in \Lambda$, where $V_{h_1,h_{k-1}} = V_{h_1} + X_{h_{k-1}}$, and Λ is index set of $X_{h_{k-1}}$ on the $(k-1)$-th level, satisfying: for any $v \in V_{h_1,h_{k-1}}$,

$$a_{h_1,h_{k-1}}(u_{h_{k-1},i}, v) - \mu_{h_{k-1}} b_{h_1,h_{k-1}}(u_{h_{k-1},i}, v) = \lambda_{h_{k-1},i}\, b_{h_1,h_{k-1}}(u_{h_{k-1},i}, v). \tag{4.9}$$

2: **Rayleigh quotient iteration**
For $s = 2, \ldots, k-1$, relax for $\widetilde{u}_{h_s,i}$ in the following source problem on level s: for any $v \in V_{h_s}$

$$a_{h_s}(\widetilde{u}_{h_s,i}, v) - \mu_{h_{k-1}} b_{h_s}(\widetilde{u}_{h_s,i}, v) = \lambda_{h_{k-1},i}\, b_{h_s,h_{k-1}}(\widetilde{u}_{h_{s-1},i}, v), \tag{4.10}$$

where $\widetilde{u}_{h_1,i} := u_{h_{k-1},i} \in V_{h_1} + X_{h_{k-1}}$.

3: **Smoothing of fine grid auxiliary source problem**
Applying a smoother for $\widetilde{u}_{h_k,i} \in V_{h_k}$ from level k back to level 1 for the following problem defined on the finest grid: for any $v \in V_{h_k}$

$$a_{h_k}(\widetilde{u}_{h_k,i}, v) - \mu_{h_{k-1}} b_{h_k}(\widetilde{u}_{h_k,i}, v) = \lambda_{h_{k-1},i} b_h(\mathcal{P}_{h_{k-1}\to h_k} \widetilde{u}_{h_{k-1},i}, v). \tag{4.11}$$

Then orthogonalize $\widetilde{u}_{h_k,i}$'s with respect to the inner product $b_{h_k}(\cdot,\cdot)$.

4: **Coarse shift and enrichment space updates**
Let $X_{h_k} = \mathrm{span}\{\widetilde{u}_{h_k,i}\}_{i\in\Lambda}$. Update the coarse grid shift μ_{h_k} based on the Rayleigh quotients of the eigenfunctions in X_{h_k}.

5: **Coarse grid eigensolve in the updated enriched space**
Find $(u_{h_k}, \lambda_{h_k}) \in V_{h_1,h_k} \times \mathbb{R}^+$ satisfying, for $i \in \Lambda$, and any $v \in V_{h_1,h_k}$:

$$a_{h_1,h_k}(u_{h_k,i}, v) - \mu_{h_k} b_{h_1,h_k}(u_{h_k,i}, v) = \lambda_{h_k,i}\, b_{h_1,h_k}(u_{h_k,i}, v). \tag{4.12}$$

where $V_{h_1,h_k} = V_{h_1} + X_{h_k}$ is the updated enriched coarse space.

Remark 4.1. For the Laplacian-Beltrami operator there are multiple eigenfunctions associated with any given nonzero eigenvalue. In the proposed multigrid scheme, for an eigenvalue with multiplicity greater than one, multiple eigenfunctions are approximated simultaneously using an eigensolve in the enriched coarse space. Note that the coarse grid approximations that are computed, $\{u_{H,i}\}_{i=1}^N$, are mutually orthogonal. However, after performing the fine grid relaxation (4.3), the $\{\widetilde{u}_{h,i}\}_{i\in\Lambda}$ are no longer orthogonal to one another. For $\widetilde{u}_{h,i}$'s associated with the same eigenvalue approximation, $\lambda_{h,k}$, a Gram-Schmidt procedure can be applied to orthogonalize them.

If $X_h = \mathrm{span}\{\widetilde{u}_{h,i}\}_{i\in\Lambda}$ contains eigenfunction approximations associated with more than one eigenvalue, then the coarse eigensolve shows numerically more robustness if the lower right block of the mass matrices in (4.8) is diagonal. Based on this observation, we use the following unconstrained trace minimization procedure (see [6]) to orthogonalize, before assembling the stiffness and mass matrices in the enriched space.

FIGURE 1. One V-cycle iteration between level 1 and level 3.

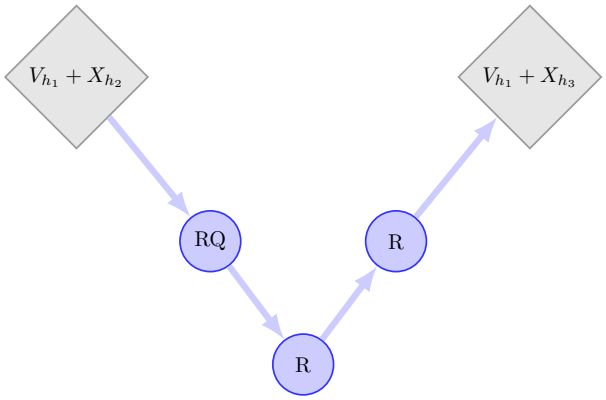

Algorithm 4 BFMG scheme for approximating eigenpairs over K levels.

1: **Coarse eigensolve**
Let $(u_{h_1,i}, \lambda_{h_1,i}) \in V_{h_1} \times \mathbb{R}^+$ $(i \in \Lambda \subset \{1, \ldots, \dim V_{h_1}\})$ solve the following eigen-problem

$$a(u_{h_1,i}, v) - \mu_{h_1} b(u_{h_1,i}, v) = \lambda_{h_1,i} b(u_{h_1,i}, v), \quad \text{for any } v \in V_{h_1}.$$

2: **V-cycle iteration**
Set a certain level $k > 1$, perform the V-cycle iteration as in Algorithm 3 between level 1 and k.

3: **Rayleigh quotient**
If $k < K$, $k \leftarrow k + 1$. If $k = K$, compute the eigenvalue approximation on the finest level for all $i \in \Lambda$ using the source approximations

$$\widetilde{\lambda}_{h_K,i} = \frac{a_{h_K}(\widetilde{u}_{h_K,i}, \widetilde{u}_{h_K,i})}{b_{h_K}(\widetilde{u}_{h_K,i}, \widetilde{u}_{h_K,i})} + \mu_{h_{K-1}}.$$

Suppose that in X_h, the set of fine grid approximations, $\{\widetilde{u}_{h,i}\}_{i\in\Lambda_j}$ correspond to eigenfunction approximations for the eigenvalues λ_{h,k_j} $(j = 1, 2)$ and assume $\lambda_{h,k_1} < \lambda_{h,k_2}$. Let the true eigenvalue counterparts satisfy $\lambda_{k_1} < \lambda_{k_2}$. Then, for every approximation solve the following unconstrained minimization problem (written in matrix form):

$$\min_{\delta U \in \mathbb{R}^{N_h \times \dim \Lambda_2}} \left\{ \operatorname{trace}\big(U^T (A_h - \lambda_{h,k_1} I) U\big) + \mu \left\| I_{\dim \Lambda} - U^T M_h U \right\|_F \right\},$$

where $U = (U_1, U_2 + \delta U)$ and μ is set to be greater than $(\lambda_{h,k_2} - \lambda_{h,k_1})/2$. Here the notation is set such that $U_j \in \mathbb{R}^{N_h \times \dim \Lambda_j}$ corresponds to the coefficients of the $\{\widetilde{u}_{h,i}\}_{i\in\Lambda_j}$ for $j = 1, 2$.

5. NUMERICAL EXPERIMENTS

In this section, we report various results from the finite element approximation of the eigenproblem (1.3) on a 2-sphere $\mathbb{S}^2$. The numerical experiments in this section are carried out using the powerful finite element toolbox *i*FEM in `MATLAB` (see [8]). The initial coarse mesh is generated by `Distmesh` (see [23]) to approximate the 2-sphere.

In all tests of both the two-grid methods (TG) and the bootstrap multigrid method (BMG), the finer meshes are obtained from a uniform refinement of the coarser mesh such that the mesh size satisfies that $h_{n-1}^4 \lesssim h_n$ between the coarser mesh at $(n-1)$-th level and the finer mesh at n-th level. The newly created vertices are then projected on to the continuous surface.

In the BMG approach, $\dim X_h$ in Algorithm 2 are fixed unless explicitly stated otherwise. This dimension is usually set as the multiplicity of the largest possible eigenvalue being computed plus some additional overlap with its neighboring eigenvalues in the discrete spectra. On the coarsest mesh, the eigen-problem is solved, and then the eigenpairs of interest form the right hand sides of the source problems that are approximated on the finer mesh. The approximate solutions obtained from the source problems are then used to enrich the coarse space, so that overall the algorithm is continuously improving the eigenpair approximations by working mainly on the coarsest level.

The true solutions to the eigen-problem (1.1) of the Laplacian-Beltrami operator on the 2-sphere are known as the real spherical harmonics (e.g. see [15]). Specifically, the j-th eigenvalues, for $l^2 \le j \le (l+1)^2 - 1$, counting multiplicity, are $\lambda_j = l(l+1)$ for $l \in \mathbb{Z}^+$. The dimension of the associated eigenspace to the l-th distinctive eigenvalue is $2l+1$.

In computation, due to the numbering of the vertices in the triangulation, the eigenfunctions obtained approximate a rotated version of the spherical harmonics represented using Cartesian coordinates. For this reason, we use a reliable and efficient a posteriori error estimator to give the error estimate of the eigenfunctions under $H^1(\Gamma)$-seminorm (energy norm associated with the bilinear form $a(\cdot,\cdot)$). The error estimator we use is a combination of the one in [10] for a non-eigen-problem, and the one from [12] for the eigen-problem on a polygonal domain. The local error estimator for a surface triangle $T \in \mathcal{T}_h$ is then as follows:

$$\eta_T^2 = h_T^2 \lambda_h^2 \left\| u_h \right\|_{L^2(T)}^2 + \frac{1}{2} \sum_{e \subset \partial T} h_e \left\| [\![\nabla_\Gamma u_h \cdot (\boldsymbol{n}_T \times \boldsymbol{\tau}_e)]\!]_e \right\|_{L^2(e)}^2 + \left\| \boldsymbol{B}_h \nabla_\Gamma u_h \right\|_{L^2(T)}^2 . \tag{5.1}$$

The first two terms measure the approximation error, and the third term measures the geometric error introduced by the triangulation. For a detailed definition of $\boldsymbol{B}_h$ please refer to [10]. We use the approach from [10] to simplify the computation of the geometric term. Namely, for any $\boldsymbol{x} \in T$, the point-wise matrix 2-norm for the geometric error operator $\boldsymbol{B}_h$ is bounded as follows for a 2-sphere $\mathbb{S}^2$:

$$\left\| \boldsymbol{B}_h(\boldsymbol{x}) \right\|_{l^2} \le \left| \frac{1 - \boldsymbol{n}(\boldsymbol{x}) \cdot \boldsymbol{n}_T(\boldsymbol{x})}{\boldsymbol{n}(\boldsymbol{x}) \cdot \boldsymbol{n}_T(\boldsymbol{x})} \right| \left(|\boldsymbol{x}|^2 + 4|\boldsymbol{x}| \right). \tag{5.2}$$

Thus the geometric part of the error can be computed by:

$$\left\| \boldsymbol{B}_h \nabla_\Gamma u_h \right\|_{L^2(T)} \le \left\| \left\| \boldsymbol{B}_h(\boldsymbol{x}) \right\|_{l^2} \right\|_{L^\infty(T)} \left\| \nabla_\Gamma u_h \right\|_{L^2(T)} , \tag{5.3}$$

where the L^∞-norm on the triangle T is computed by comparing the values of $\left\| \boldsymbol{B}_h(\boldsymbol{x}) \right\|_{l^2}$ at the three vertices this triangle has. Finally the global error estimator is obtained by $\eta(u_h) := \left(\sum_{T \in \mathcal{T}_h} \eta_T^2 \right)^{1/2}$.

5.1. **Standard two-grid eigensolver.** To begin with, we apply the two-grid method from Algorithm 1 with shift $\mu = 0$, wherein the indefinite shifted problem is solved directly. Our aim is to illustrate the spectra loss phenomenon that is caused by a coarse space being too small. To this end, the coarsest mesh that approximates the sphere is set to have only 54 nodes, i.e., $\#(\texttt{DoF}_H) = 54$. The coarsest spectrum computed by `eigs` can be viewed in Figure 2a. We can observe that the true $\lambda_j = 30$ for $26 \le j \le 36$, and the dimension of the eigenspace for

$\lambda_j = 30$ is 11. Further, we see that the numerical approximations to the higher end of the spectrum have large errors, that is, we see that the approximated $\lambda_{H,j}$ on the coarse mesh are closer to the next eigenvalue 42 in the spectra than the true eigenvalue 30 they are supposed to approximate. This causes part of the eigenpairs from the coarse eigenspace $M(\lambda_{H,j})$ for $26 \leq j \leq 36$ to converge to eigenpairs of the true $\lambda_{j'} = 42$ for $37 \leq j' \leq 49$. As a result, as seen in Figure 2b $\dim(M(\lambda_{h,j})) = 8 < \dim(M(\lambda_j)) = 11$, where $M(\lambda_{h,j})$ is the finite element approximated eigenspace associated with $\lambda_{h,j} \approx 30$.

Note that the spectrum loss becomes even more severe for the approximation of the eigenspace for the true eigenvalue $\lambda_j = 42$ ($37 \leq j \leq 49$). In this case, if we use the same coarse mesh only four eigenfunctions are recovered for the approximated eigenspace (see Figure 2b).

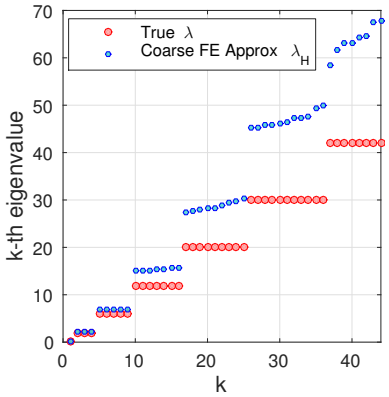

(A) Coarse grid approximation λ_H's versus the true λ.

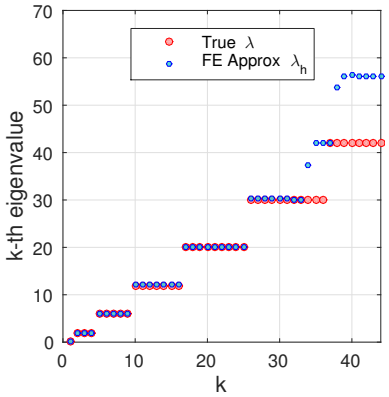

(B) Two-grid approximation λ_h's after 5 levels versus the true λ.

FIGURE 2. Coarse $\#(\texttt{DoF}_H) = 54$. TG method results in the approximated eigenspace dimension being less than intended. Blue dots are the Rayleigh quotients computed by the two-grid finite element approximations. Red dots are true eigenvalues.

When a certain eigenpair is lost in the two-grid approximation scheme, a finer coarse mesh can be used in order to recover an improved approximation. This is because on a finer coarse mesh the wavelength of these eigenfunctions can be resolved. As an example consider the case where the coarse mesh $\#(\texttt{DoF}_H) = 54$ and the 34-th eigenvalue ($\lambda_{34} = 30$) is wrongly approximated by the two-grid method (see Figure 2b). If a finer coarse mesh is used instead with $\#(\texttt{DoF}_H) = 96$, then the 34-th eigenvalue is recovered. A comparison of this case is provided in Figure 3.

5.2. **Bootstrap multigrid enrichment.** An alternative to simply increasing the coarse space by refining the mesh is given by the bootstrap idea to enrich the coarse space with eigen-approximations obtained by solving source problems on finer meshes. If the dimension of the coarsest enriched space is fixed such that $\dim V_H + 1$ (as in the method from [19]), then approximating larger eigenvalues with multiplicity greater than one still requires a finer coarse space.

To see this we consider the case where the user wants to recover the eigenvalues that corresponds to $\lambda_j = 42$ where $37 \leq j \leq 49$. In this example, the coarsest space $V_H = V_{h_1}$ is chosen

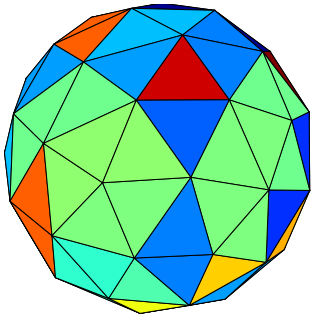

(A) #DoF = 54, u_H with $\lambda_{H,34} \approx 47.5871$.

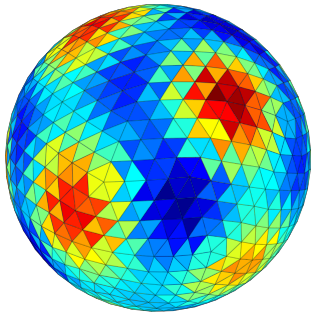

(B) After 3 levels of refinement, $\lambda_{h,34} \approx 39.7353$, u_h is visually an approximation to an eigenfunction associated with $\lambda_j = 42$ $(37 \leq j \leq 49)$.

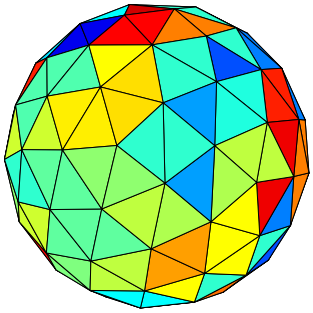

(C) #DoF = 96, u_H with $\lambda_{H,34} \approx 40.8393$.

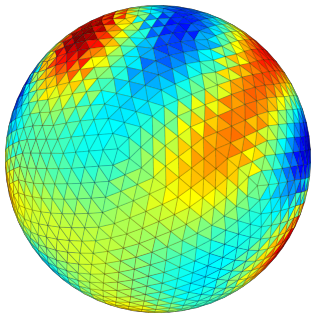

(D) After 3 levels of refinement, $\lambda_{h,34} \approx 30.6344$, correct approximation u_h to an eigenfunction associated with $\lambda_j = 30$ $(26 \leq j \leq 36)$.

FIGURE 3. Two-grid method, comparison of finite element approximations of one eigenfunction associated with eigenvalue $\lambda_{34} = 30$ starting from different coarse meshes.

as in the previous example where $\#(\texttt{DoF}_H) = 54$. We set the coarse space being enriched as $V_{h_1,h_2} := V_{h_1} + \{\widetilde{u}_{37,h_2}\}$, and solve the coarse eigen-problem using `eigs` in Matlab. The results in Figure 4a show that the new approximation $\lambda_{h_2,37}$ does approximate the 37-th eigenvalue to some extent. However, when we perform this procedure again and then solve the coarse eigen-problem in the updated enriched space $V_{h_1,h_3} := V_{h_1} + \{\widetilde{u}_{37,h_3}\}$, we observe that the approximation to the eigenpair of interest does not improve (see Figure 4b).

The reason for this behavior can be explained as follows. First, we see that the approximations to $\lambda_{h_1,j}$ $(26 \leq j \leq 36)$ are closer to the true eigenvalue $\lambda_j = 42$ $(37 \leq j \leq 49)$ than the corresponding discrete spectra $\lambda_{h_1,j}$ $(37 \leq j \leq 49)$. As the coarse space is enriched by a single function $\{\widetilde{u}_{h_2,37}\}$, which is obtained by solving a single source problem in V_{h_k} $(k \geq 2)$ on the k-th level, the new approximation $\lambda_{h_k,37}$ becomes closer to the true eigenvalue $\lambda_{37} = 42$ that it is supposed to approximate. However, it is still not as good an approximation as $\lambda_{h_1,j}$

$(26 \leq j \leq 36)$ to the true eigenvalue $\lambda_{37} = 42$. As such, the algorithm mixes these modes and then can not detect the eigenpair of interest.

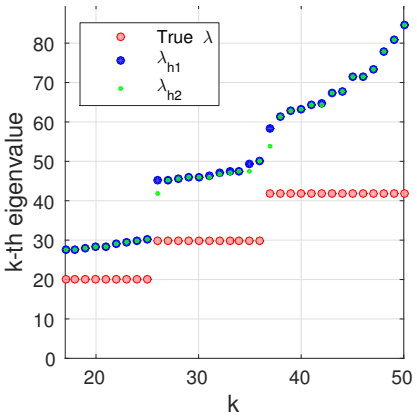

(A) Coarse eigensolve approximations λ_{h_1}, and λ_{h_2} obtained from solving a coarse eigen-problem in an enriched space $V_{h_1} + \{\tilde{u}_{h_2}\}$, versus the true λ.

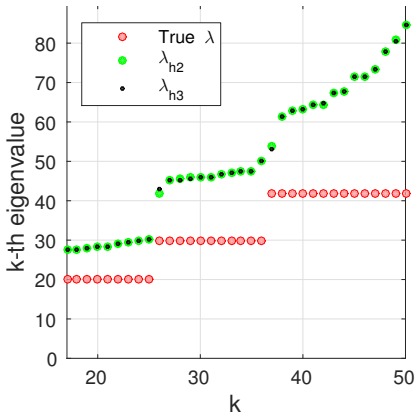

(B) λ_{h_2} obtained from $V_{h_1} + \{\tilde{u}_{h_2}\}$, and λ_{h_3} obtained from $V_{h_1} + \{\tilde{u}_{h_3}\}$, versus the true λ.

FIGURE 4. Coarse $\#(\texttt{DoF}_H) = 54$, single enrichment multigrid method results in the eigenpair of interest not being represented in the discrete spectrum. Red dots are true eigenvalues.

Heuristically speaking, for the Laplace Beltrami eigenvlaue problem on the sphere, assuming the a priori knowledge of the dimension of the eigenspace, it follows that if we seek to approximate the l-th distinctive eigenvalue $\lambda_j = l(l+1)$, then the coarse space V_{h_1} should at least be enriched by the subspace $X_{h_k} = \text{span}\{\widetilde{u}_{h_k,j'}\}_{j' \in \Lambda}$, where $\Lambda = \{j' \in \mathbb{Z} : (l-1)^2 + 1 \leq j' \leq j\}$. In this example, for $\lambda_{37} = 42$ where $l = 7$, the enrichment space X_{h_k} is $\text{span}\{\widetilde{u}_{h_k,j'}\}_{26 \leq j' \leq 37}$, where the $\widetilde{u}_{h_k,j'}$'s denote the solutions to the source problems in the finer space V_{h_k} on the k-th level $(k \geq 2)$ for the 26-th to 37-th eigenpairs of the discrete spectra. The comparison can be found in Figure 5a, 5b. Now, because the discrete eigenvalues $\lambda_{h_k,j}$ $(26 \leq j \leq 36)$ are better approximated after the coarse space is enriched with multiple eigenfunctions, the algorithm is able to better detect the eigenpair of interest $\lambda_{h_k,j}$ $(j = 37,\ k = 2, 3)$ after the second coarse eigensolve, and overall we see that the approximations improve.

If one is interested in recovering all the eigenvalues from the smallest one, then Algorithm 2 can be applied with an index-fixed X_{h_k}, and for each distinctive eigenvalue one at a time. Here we choose a fixed dimension 20 (greater than the biggest numerical multiplicity observed from the coarse eigensolve). The 20 enrichment candidate functions are the eigenfunctions associated with the 20 eigenvalues nearest to the eigenvalue of interest on the discrete spectra, and these eigenfunctions are kept through the BFMG cycle in X_{h_k} (level $k = 2, 3, 4$). The discrete spectra recovered using this setting can be found in Figure 6a and Figure 7.

Another benefit of the bootstrap enrichment idea is that increasingly larger eigenvalues can be recovered from the eigensolve in the continuously updating enriched coarse space of fixed size. Using the same setting as the above example, the enrichment space X_{h_k} is now set to be of dimension 17 on the k-th level and its elements are the solutions to the source problems, where

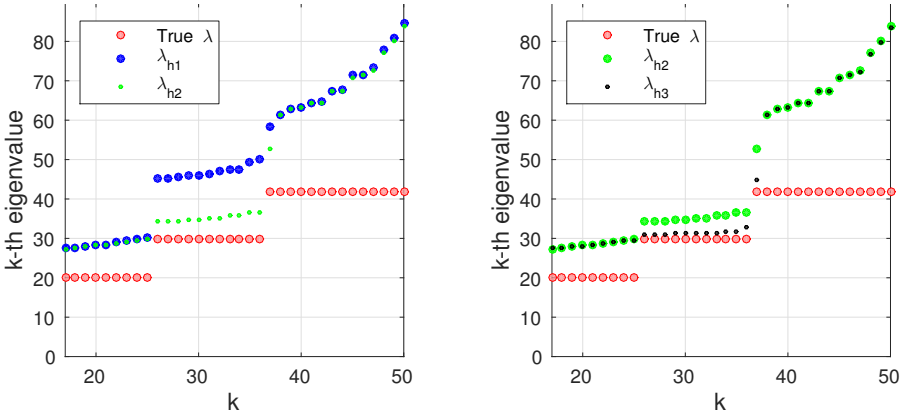

(A) Coarse grid eigensolve approximations λ_{h_1}'s, and λ_{h_2}'s obtained from the eigensolve in the enriched space $V_{h_1} + \text{span}\{\widetilde{u}_{h_2,j'}\}_{26\le j'\le 37}$, versus the true λ.

(B) Enriched coarse eigensolve approximations λ_{h_2}'s obtained from $V_{h_1} + \text{span}\{\widetilde{u}_{h_2,j'}\}_{26\le j'\le 37}$, and λ_{h_3}'s obtained from $V_{h_1} + \text{span}\{\widetilde{u}_{h_3,j'}\}_{26\le j'\le 37}$, versus the true λ.

FIGURE 5. Coarse $\#(\texttt{DoF}_H) = 54$, the enrichment space is chosen according to the placement of the eigenpair of interest on the discrete spectra. Red dots are true eigenvalues.

the right sides are generated from the eigenfunctions associated with the largest 17 eigenvalues coming from the eigensolve on the coarsest level. In this scenario, the enrichment space X_{h_k} changes on the different levels.

After 4 levels of this bootstrapping procedure, all 13 eigenfunctions associated with $\lambda_j = 42$ $(37 \le j \le 49)$ are correctly approximated. Moreover, 11 eigenfunctions out of 15 associated with $\lambda_j = 56$ $(50 \le j \le 64)$, and 8 eigenfunctions associated with $\lambda_j = 72$ $(65 \le j \le 81)$ are recovered (see Figure 6b). These results are further demonstrated in Figure 10. Figure 10 corresponds to the approximation obtained from taking 67th eigenfunction produced by the eigensolve on this enriched coarse space and interpolating and relaxing on the source problem (4.3) until the 4th level is reached. Note that the resulting approximation now approximates the eigenfunction associated with $\lambda = 72$.

The other way of improving the eigenvalue approximation for a certain range is to set a shift $\mu > 0$ in Algorithm (2) to achieve a "zoom in" effect. In Figure 8a, a coarse grid shift $\mu_{h_1} = 32$ is applied in the coarse solve in Algorithm 2. The enrichment candidate space X_{h_1} is chosen to be a fixed dimension of 20, using the 20 eigenfunctions associated with the 20 eigenvalues closest to 0. After the source solves in V_{h_2}, when performing the eigensolve in an enriched coarse space $V_{h_1,h_2} = V_{h_1} + X_{h_2}$, the new coarse grid shift μ_{h_2} is set to be the previous shift μ_{h_1} plus the average of the Rayleigh quotients of the functions in X_{h_2}, which contain all the source solutions from problem (4.3) using functions from X_{h_1} as the sources. This averaging for the new shift is ad-hoc. The reason for this choice is that we observe in practice that performing the BMG procedure brings the discrete spectra closer to the true spectra, consequently, the averaging after each V-cycle is to compensate for this change. When this procedure is repeated twice between level 3 to level 1 and between level 4 to level 1, the result is in Figure 8b. The

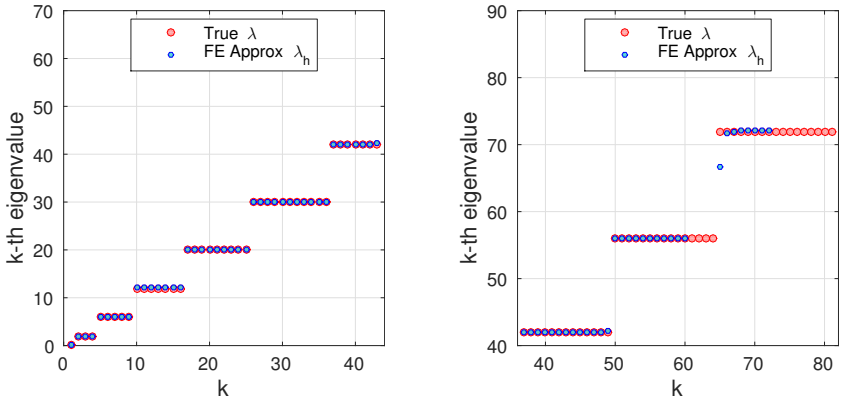

(A) Multigrid approximations λ_h's after 4 levels versus the true λ.

(B) Multigrid approximations λ_h's after 6 levels versus the true λ.

FIGURE 6. Coarse $\#(\texttt{DoF}_H) = 54$. BMG with a index-fixed enrichment space of dimension 20 converges as intended (left). BMG with an index-updating enrichment space is able to detect higher eigenvalues that can not be resolved in the coarse grid (right). Blue dots are the Rayleigh quotient computed by the multigrid finite element approximations. Red dots are true eigenvalues.

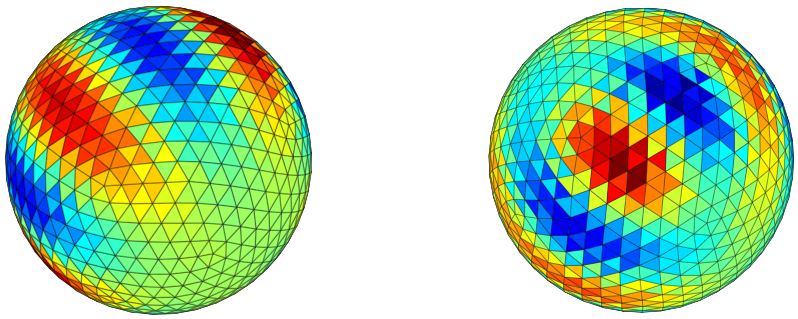

(A) $\#\texttt{DoF} = 3330$, $\lambda_{h_4,34} \approx 30.3061$, correct approximation u_h to an eigenfunction associated with $\lambda_j = 30$ $(26 \leq j \leq 36)$.

(B) $\#\texttt{DoF} = 3330$, $\lambda_{h_4,42} \approx 42.4909$, correct approximation u_h to an eigenfunction associated with $\lambda_j = 42$ $(37 \leq j \leq 49)$.

FIGURE 7. The BMG results of the finite element approximations of the eigenfunction associated with eigenvalues $\lambda_{34} = 30$ and $\lambda_{37} = 42$ after 4 levels of refinement starting with $\#\texttt{DoF} = 54$ (Figure shows solutions on the 3rd level). Note for TG, these approximations can only be recovered correctly with $\#\texttt{DoF} = 96$.

convergence after 5 levels of refinement can be found in Figure 9. We note that if the shift is unchanged after each V-cycle, then a similar phenomenon as in Figure 4b is observed.

Another interesting observation is that by computing the enrichment space according to the eigenpairs that we are attempting to approximate we are able to obtain improved approximations to these interior eigenvalues without having to first compute accurate approximations

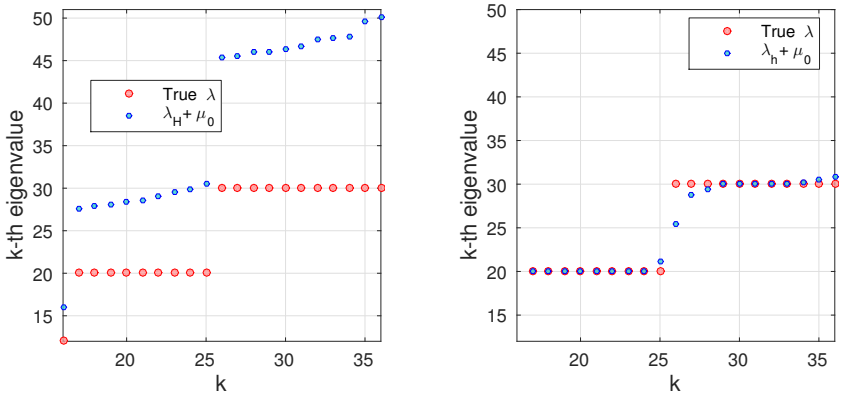

(A) Coarse grid approximation λ_{h_1}'s, the shift $\mu_{h_1} = 32$.

(B) λ_{h_4}'s obtained from $V_{h_1} + X_{h_4}$, the shift $\mu_{h_4} = 24.9861$.

FIGURE 8. Coarse $\#(\texttt{DoF}_H) = 54$, both the enrichment space and the shift μ are chosen on each level based on the current approximation to the eigenpair of interest on the discrete spectra. Red dots are true eigenvalues.

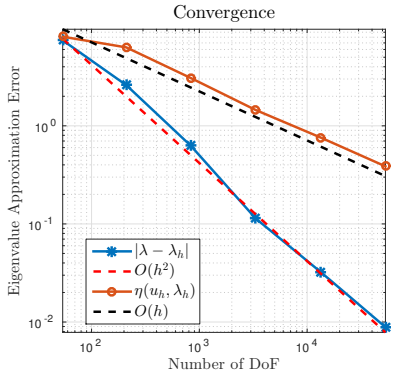

FIGURE 9. Convergence results of BMG using the shifted problem with an updating μ to approximate interior eigenvalue $\lambda = 20$. The enrichment space's dimension is 20 where the eigenfunctions of the 20 eigenvalues nearest to 0 are used. The coarse eigensolve is performed with a shift updated after each BMG V-cycle 3. The convergence is plotted for the smallest eigenvalue among the ones which approximate $\lambda = 20$.

to the smaller eigenvalues and their corresponding eigenfunctions (see Figure 5b). Thus, the BMG approach can be used to compute interior eigenpairs. In contrast, the approach proposed in [6] only computes multiple eigenpairs starting with the smallest. In this way, our method for the shifted Laplace-Beltrami eigen-problem is more general and flexible than this and other previous methods that have been developed for the Laplace eigen-problem on the plane.

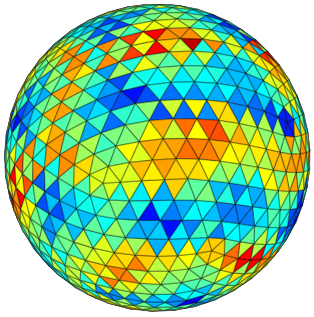

(A) 67th eigenfunction from the coarse eigensolve interpolated to the 3rd level. The coarse space has $\#\texttt{DoF} = 54$, and is enriched by space X_{h_3} containing the 15 eigenfunctions associated with the largest eigenvalues from the eigensolve.

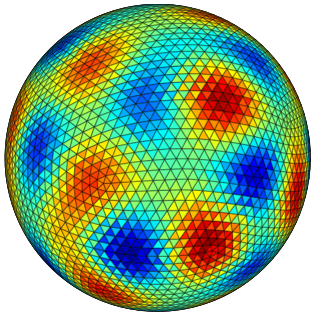

(B) The source problem solution on the 4th level, obtained by relaxing the source problem using the 67th eigenfunction from the coarse eigensolve, is an approximation to the eigenfunction associated with $\lambda = 72$.

FIGURE 10. The bootstrapping multigrid procedure results higher eigenmodes to be detected in the coarsest space.

5.3. **Solving versus relaxing the source problem.** In previous works on designing multigrid eigensolvers (e.g. [19, 25]), the auxiliary problems in the correction step are solved with a direct method on the fine level. In the BMG algorithm, the exact solve is replaced with an iterative solver (a smoother such as Gauss Seidel). We illustrate in the numerical experiments that a direct solve of the shifted and indefinite system is not necessary, and that relaxation on the shifted source problems suffices to guarantee the optimal convergence rate for the approximation of the eigenpair the algorithm produces. In all tests, we set the shift in BMG to be $\mu = 0$. To approximate the unshifted positive definite source problems (4.3) of BMG on the k-th level, 1 BMG V-cycle (Step 3 in 3) is applied with 1 sweep of Gauss-Seidel smoother per level. While for the shifted problem (3.3)(indefinite) of TG method, 1 V-cycle with 5 sweeps of Kacmarcz smoother per level is applied. Note that this simplification reduces the overall computational cost of the approach significantly.

In Table 1, we compare the rate of convergence for the approximation of the first three distinct eigenvalues, using an exact solve versus using relaxation in the two-grid method (TG) and bootstrap multigrid (BMG) method respectively. In the table, the entries are the rates of convergence r, so that $|\lambda - \lambda_{h_k}| \sim O(\#(\texttt{DoF}_k)^{-r})$ where k stands for the current level. Note that, the optimal rate of convergence of $O(h_k^2)$ for the eigenvalue approximation is achieved with $r \approx 1$. The first column in Table 1, contains the true eigenvalues. The second and the fourth columns give the value of r for the TG and the BMG methods when the indefinite shifted problem is solved directly. The third and the last columns correspond to the TG and BMG methods where a smoother is applied to the source problems on the finer levels.

The experiments correspond to 3 choices of the eigenvalues and the results suggest that it is sufficient to solve the unshifted source problem using Gauss Seidel and the BMG method still yields a nearly optimal rate of convergence with $r \approx 1$. In addition, the promising two-grid results obtained using the Kaczmarz iteration for the indefinite system togehter with the multilevel results reported in the previous section for the shifted (indefinite) Laplace Beltrami

eigen-problem suggest that the algorithm will also work well for symmetric indefinite problems such as the Helmholtz equation.

λ	TG	TG w/ Kaczmarz	BMG	BMG w/ GS
2	1.0084	0.9656	1.0037	0.9963
6	1.0063	0.9575	1.0005	0.9764
12	1.0084	0.9731	1.0059	0.9801

TABLE 1. Comparison of the rates of convergence $O(\#(\texttt{DoF})^{-r})$.

The convergence rates of the BMG algorithm with uniform refinement are further verified numerically for the Laplace-Bertrami eigen-problem on the sphere in Figure 11. These results are on par with the TG estimates (3.9). Note that for larger eigenvalues, *e.g.*, $\lambda_j = 30$ (plot on the right) more degrees of freedom are needed in order to obtain the same accuracy as for smaller eigenvalues, *e.g.*, $\lambda = 2$ (plot on the left). Of course, the resolution required to achieve high accuracy for large eigenvalues is expected to be greater since these modes are generally more oscillatory. The key difference in the BMG algorithm is that with the enriched coarse space it is possible to approximate larger eigenvalues without needing to continuously increase the size of the coarsest system in order to approximate larger eigenmodes, as required by the standard two-grid method.

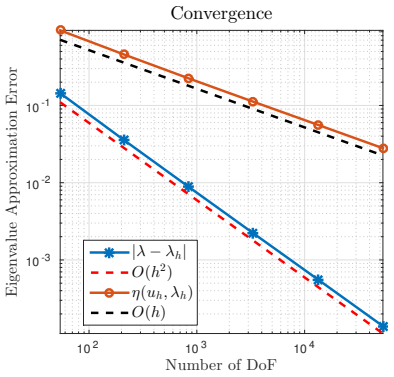

(A) $\lambda = 2$. The enrichment space's dimension is fixed to be 6 using the 6 eigenfunctions of the lowest 6 eigenvalues from the coarse eigensolve.

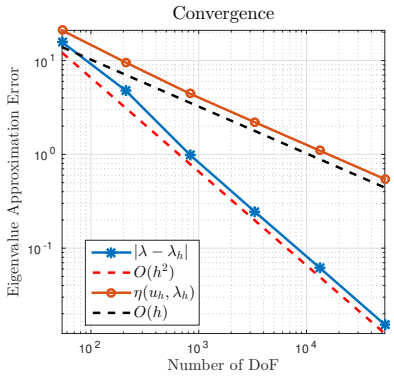

(B) $\lambda = 30$. The enrichment space's dimension is fixed to be 15 using the 15 eigenfunctions of the 15 eigenvalues starting from the 20-th eigenvalue from 0.

FIGURE 11. Convergence results of BMG: using unshifted problem to approximate $\lambda = 2$, $\lambda = 30$.

6. CONCLUSIONS

In this paper, we designed and analyzed a finite element bootstrap multigrid method for solving the shifted Laplace-Beltrami eigen-problem. Our analysis and numerical experiments

focused mainly on this model problem since the true solutions are known, allowing us to systematically study the performance of the algorithm.

We extended the standard two-grid method from [16] for the Laplace eigen-problem on the plane to the shifted Laplace-Beltrami eigen-problem on a surface and we showed that the method gives optimal ($O(h^2)$) convergence, assuming that the coarsening is not too aggressive and that the coarse eigen-problem is solved using a direct method. We also showed that if the coarse mesh is not fine enough then a spectra loss phenomena occurs and that approximating larger eigenvalues requires increasingly finer coarse meshes. This in turn results in a suboptimal algorithm since the coarse eigen-problem has to be solved to high accuracy in order to maintain optimal convergence.

To treat the spectral loss observed in the standard two-grid algorithm, we introduced a bootstrap method that enriches the coarse space with a subspace consisting of increasingly accurate approximations to the eigenmodes of interest. These approximations are computed by applying a few steps of relaxation to a symmetric source problem. We showed that the bootstrap approach is able to approximate eigenmodes with large multiplicity provided that the enrichment space has sufficiently large dimension. Generally, the dimension of the coarsest space depends on the dimension of the eigenspace that the user wants to compute, but it does not depend on which eigenpair is being approximated. We note that in cases where high dimensional enrichment subspaces are required to solve a given problem, multiple coarse spaces can be used in order to improve the efficiency of the overall algorithm.

We showed that the bootstrap eigensolver can be used to compute a large portion of the eigenspace, starting with the smallest eigenmodes. We also showed that if instead only a few large eigenmodes are sought, then shifted indefinite systems can be solved using the BMG algorithm with Kaczmarz smoother in order to compute interior eigenpairs directly.

In the numerical experiments, uniform refinement are adopted in all cases. Of course, an adaptive finite element method would give a more robust and efficient approach (e.g., for problems with singularities or when only interior eigenvalues are needed) and can be used in practice. Combining the approach with adaptive surface finite element method in [10] is a topic of our current research.

References

[1] Ivo Babuška and John E Osborn. Finite element-Galerkin approximation of the eigenvalues and eigenvectors of self-adjoint problems. *Mathematics of computation*, 52(186):275–297, 1989. 5, 6, 8

[2] Daniele Boffi. Finite element approximation of eigenvalue problems. *Acta Numerica*, 19(1):1–120, 2010. 6

[3] A. Brandt, J. Brannick, K. Kahl, and I. Livshits. Bootstrap AMG. *SIAM Journal of Scientific Computing*, 33:612–632, 2011. 2, 11, 12

[4] J. Brannick and K. Kahl. Bootstrap algebraic multigrid for the 2D Wilson-Dirac system. *SIAM Journal of Scientific Computing*, 36(3):321–347, 2014. 2

[5] Z. Cai, J. Mandel, and S. McCormick. Multigrid methods for nearly singular linear equations and eigenvalue problems. *SIAM Journal on Numerical Analysis*, 34:178–200, 1997. 2

[6] Tony F Chan and Ilya Sharapov. Subspace correction multi-level methods for elliptic eigenvalue problems. *Numerical linear algebra with applications*, 9(1):1–20, 2002. 2, 3, 13, 21

[7] Isaac Chavel. *Eigenvalues in Riemannian geometry*, volume 115. Academic press, 1984. 4

[8] Long Chen. *i*FEM: an innovative finite element methods package in MATLAB. 2008. 14

[9] Philippe Clément. Approximation by finite element functions using local regularization. *Revue française d'automatique, informatique, recherche opérationnelle. Analyse numérique*, 9(2):77–84, 1975. 5

[10] Alan Demlow and Gerhard Dziuk. An adaptive finite element method for the Laplace-Beltrami operator on implicitly defined surfaces. *SIAM Journal on Numerical Analysis*, 45(1):421–442, 2007. 3, 4, 5, 6, 10, 15, 24

[11] Jozef Dodziuk. Finite-difference approach to the hodge theory of harmonic forms. *American Journal of Mathematics*, pages 79–104, 1976. 5

[12] Ricardo G Durán, Claudio Padra, and Rodolfo Rodríguez. A posteriori error estimates for the finite element approximation of eigenvalue problems. *Mathematical Models and Methods in Applied Sciences*, 13(08):1219–1229, 2003. 15

[13] Gerhard Dziuk. Finite elements for the beltrami operator on arbitrary surfaces. In Stefan Hildebrandt and Rolf Leis, editors, *Partial Differential Equations and Calculus of Variations*, volume 1357 of *Lecture Notes in Mathematics*, pages 142–155. Springer Berlin Heidelberg, 1988. 4, 5

[14] Gerhard Dziuk and Charles M Elliott. Finite element methods for surface PDEs. *Acta Numerica*, 22:289–396, 2013. 1, 3, 4

[15] Ernest William Hobson. *The theory of spherical and ellipsoidal harmonics*. CUP Archive, 1955. 15

[16] Xiaozhe Hu and Xiaoliang Cheng. Acceleration of a two-grid method for eigenvalue problems. *Math. Comp.*, 80:1287–1301, 2011. 1, 3, 8, 9, 24

[17] Michael Kaschiev. An iterative method for minimization of the Rayleigh Ritz functional. *Computational Processes and Systems*, 6:160 170, 1988. 2, 3

[18] Mats G Larson. A posteriori and a priori error analysis for finite element approximations of self-adjoint elliptic eigenvalue problems. *SIAM journal on numerical analysis*, 38(2):608–625, 2000. 5

[19] Qun Lin and Hehu Xie. A multi-level correction scheme for eigenvalue problems. *Mathematics of Computation*, 84(291):71–88, 2015. 2, 3, 16, 22

[20] Sergei Maliassov. On the analog of schwarz method for spectral problems. *Numerical methods and mathematical modeling*, page 70 79, 1992. 2, 3

[21] Mark Meyer, Mathieu Desbrun, Peter Schröder, and Alan H Barr. Discrete differential-geometry operators for triangulated 2-manifolds. In *Visualization and mathematics III*, pages 35–57. Springer, 2003. 5

[22] Maxim A Olshanskii and Arnold Reusken. A finite element method for surface PDEs: matrix properties. *Numerische Mathematik*, 114(3):491–520, 2010. 1

[23] Per-Olof Persson and Gilbert Strang. A simple mesh generator in MATLAB. *SIAM Review*, 46(2):329–345, 2004. 14

[24] Ulrich Pinkall and Konrad Polthier. Computing discrete minimal surfaces and their conjugates. *Experimental mathematics*, 2(1):15–36, 1993. 5

[25] Milena R Racheva and Andrey B Andreev. Superconvergence postprocessing for eigenvalues. *Computational Methods in Applied Mathematics Comput. Methods Appl. Math.*, 2(2):171–185, 2002. 22

[26] Richard Schoen and Shing-Tung Yau. *Lectures on differential geometry*, volume 2 of *Conference Proceedings and Lecture Notes in Geometry and Topology*. I. International Press, Cambridge, MA, 1994. 2

[27] Huayi Wei, Long Chen, and Yunqing Huang. Superconvergence and gradient recovery of linear finite elements for the Laplace-Beltrami operator on general surfaces. *SIAM Journal on Numerical Analysis*, 48(5):1920–1943, 2010. 1, 3

[28] J. Xu and A. Zhou. A two-grid discretization scheme for eigenvalue problems. *Math. Comp.*, 70:17–25, 1999. 1, 3

[29] J. Zhou, X. Hu, L. Zhong, S. Shu, and L. Chen. Two-grid methods for maxwell eigenvalue problems. *SIAM Journal on Numerical Analysis*, 52(4):2027–2047, 2014. 1, 6, 9

Department of Mathematics, Pennsylvania State University, University Park, State College, PA 16802

E-mail address: brannick@psu.edu

Department of Mathematics, Pennsylvania State University, University Park, State College, PA 16802

E-mail address: scao@psu.edu